IEEE Access
Multidisciplinary | Rapid Review | Open Access Journal

Received July 13, 2021, accepted September 3, 2021, date of publication September 7, 2021, date of current version November 9, 2021.

Digital Object Identifier 10.1109/ACCESS.2021.3111097

Improving Contrast Accuracy and Resolution of Laser Speckle Contrast Imaging Using Two-Dimensional Entropy Algorithm

XINGLONG LIU[1], HUI YANG[1], AND RAN LI[2]
[1]School of Optical-Electrical and Computer Engineering, University of Shanghai for Science and Technology, Shanghai 200093, China
[2]School of Medical Instrument and Food Engineering, University of Shanghai for Science and Technology, Shanghai 200093, China

Corresponding authors: Hui Yang (yanghui@usst.edu.cn) and Ran Li (ran89@usst.edu.cn)

This work involved human subjects or animals in its research. Approval of all ethical and experimental procedures and protocols was granted by Hospital Ethics Committee.

ABSTRACT A two-dimensional entropy laser speckle contrast imaging (E-LSCI) algorithm is proposed to improve the accuracy and resolution of laser speckle contrast imaging (LSCI) systems. Owing to the stable characteristics of two-dimensional entropy in speckle images, it can be used as a reference to correct contrast. E-LSCI introduces two-dimensional entropy into the contrast ratio calculation. It uses this benchmark and performs normalization to obtain a more accurate contrast ratio. The results of the method validation experiment show that the accuracy and contrast resolution of E-LSCI are higher than those of traditional LSCI by 27% and over 80%, respectively. The results of a finger blocking experiment show that E-LSCI can reduce the variance of contrast ratio at an identical flow velocity and improve the resolution by 25%. The application of this algorithm can improve the contrast accuracy and contrast resolution of laser speckle contrast imaging instruments.

INDEX TERMS Laser speckle contrast imaging, speckle contrast analysis, image two-dimensional entropy, contrast accuracy, contrast resolution.

I. INTRODUCTION

Microcirculation vascular dysfunction is generally associated with diseases such as pseudoxanthoma elastica, mild cognitive impairment, Alzheimer's disease, cholecystitis, obesity, and hypertension [1]–[5]. As a modern imaging technique with high space-time resolution [6]–[10], laser speckle contrast imaging (LSCI) is capable of non-contact, real-time, and non-invasive monitoring of capillary blood vessels and their relative blood flow variations in human tissues. This technique has gradually replaced laser Doppler as a tool for studying skin microcirculation because of its advantages such as large area, high resolution, short time consumption, and low variability [11]. In addition, it has a significant advantage in terms of miniaturization and portability because it does not combine mechanical scanning and simple structural characteristics [12]–[15]

The contrast resolution of a LSCI system is of considerable importance. In addition, the accuracy of speckle contrast analysis exerts a significant influence on the quality of blood flow imaging. Several researchers have conducted studies with a focus on improving the contrast resolution. In this regard, there are two commonly used methods. The first method involves obtaining better experimental conditions using physical methods. For example, Zhang *et al.* [16] used an improved dual-laser experimental device to compare and analyze the scattering effects of different laser wavelengths to enhance the accuracy of the substrate ratio. However, dual-laser devices are more complex and are not conducive to popularization. The weighted average calculation of multiple speckle images obtained can enhance the contrast image results to a certain extent by altering the spatial coherence of the light source with a cylindrical lens (such as that by He *et al.* [17]). However, this method requires relatively complex experimental conditions, and more uniform and accurate experimental equipment and equipment construction effects. In addition, it displays low portability. The second method

The associate editor coordinating the review of this manuscript and approving it for publication was Sabah Mohammed.

involves improving the software algorithm. For example, Cheng *et al.* [18] proposed an effective non-local filtering strategy based on block matching and a three-dimensional transform domain. It effectively addressed the noise problem in images. However, it did not improve the contrast accuracy of a low flow-speed. A few scholars [19]–[21] have proposed linear correction of contrast values by comparing the ratios of the areas of interest and the largest and smallest backgrounds or by comparing the ratios of different flow velocities, to obtain better contrast resolution. However, neither of these can be used as a benchmark for the contrast ratio of the same system because of the large fluctuations in contrast accuracy and contrast resolution.

Because the contrast ratio is calculated by the degree of image blur, image entropy is used by scholars to reflect the degree of image blur and express the corresponding velocity information in the laser speckle image. Humeau-Heurtier *et al.* [22] introduced the concept of multiscale entropy into laser speckle systems to improve the accuracy of contrast ratios by increasing the time series. However, this method is not used widely because of its excessive calculation time and instability. Miao *et al.* [23] used image entropy to calculate images according to the results of laser speckle contrast analysis. Although the results of this method were similar to those of the traditional contrast algorithm in terms of the accuracy and resolution of marginal flow velocity difference, a method of entropy calculation was introduced. Furthermore, a new direction was proposed for the analysis of laser speckle images.

In this study, a two-dimensional entropy feature was introduced into the entropy LSCI (E-LSCI) image to correct the low contrast resolution and low accuracy and thereby, improve the correlation between the speckle contrast and relative flow velocity. The hose simulation experiment verified that the E-LSCI algorithm significantly improved the contrast accuracy and contrast resolution. Furthermore, the finger block experiment verified the effectiveness of the current E-LSCI algorithm in the microcirculation example.

II. EXPERIMENTAL SYSTEM AND METHOD

A. BASIC EXPERIMENTAL SYSTEM

The LSCI system is shown in Figure 1. The study uses a fiber laser with a homogenization lens (wavelength = 808 nm; power = 200 mw; power stability <3%; spot homogenization effect >80%; product model: FC -808-2000-MM; supplied by Shanghai Xilong Optoelectronics Co., Ltd.) to obtain a light source with uniform speckle and stable light intensity. The laser was broadened by a homogenizing lens and illuminated on the measured area through a polarizing mirror. Thereby, an adjustable spot with a diameter of 20 cm was obtained. To ensure imaging accuracy, in this study, 1) the Baumer VLG CCD camera (resolution 1932 × 1040; A/D digits 8 bit; supplied by Baumer) is used and 2) the bit depth of the image is 8 bit (0–255 gray value). The speckle image to be measured was acquired using a near-infrared CCD camera after being passed through a polarizer and

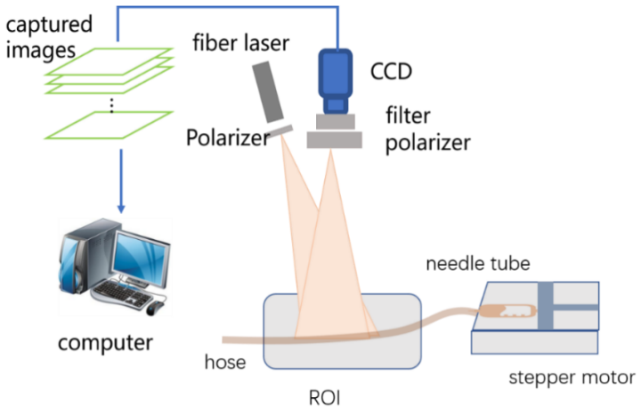

FIGURE 1. Schematic of hose experimental device.

a filter. During the testing, the vertical distance between the CCD camera and measurement area was 60 cm and that between the exit of the laser source and the object to be measured was 70 cm. These ensured that the polarized laser could uniformly cover the imaging range of the CCD. In all the experiments, the exposure time of the CCD was 20 ms. Polarizers and filters remove the interference caused by reflected light and light of other wavelengths. The filter used in the imaging system was an 810BP30OD3T90N01 narrowband filter. The center frequency of the filter was 810 nm, the light transmittance T > 90% in the bandwidth of 30 nm, the filter range was 200–1200 nm, and the cutoff band transmittance was 0.001. All the experiments in the study were carried out under identical experimental conditions and used the above-mentioned system for data collection.

To verify the effect of the contrast ratio method, the study used the hose experiment to test and compare the accuracy and resolution standards [24]. The installation diagram of the hose test is shown in Fig. 1. The inner and outer diameters of the hose were 10 mm and 13 mm, respectively. The liquid in the hose was 2% milk with a particle size of 5–10 um. It was observed experimentally that the size of the inner diameter of the hose exerted less influence on the measurement result of the liquid flow speed of the contrast ratio. A larger inner diameter can result in a more stable liquid-flow speed state. The average velocity of microcirculation was 0.7 mm/s. The velocity of blood in the local blood vessel was significantly low (0.41 mm/s). To verify the monitoring effect of the contrast ratio method on the flow velocity, the study used a stepper motor to vary the flow velocity from low to high. That is, the flow velocity of the liquid in the tube was increased from 0.4 mm/s to 1.2 mm/s, and the flow velocity difference was 0.1 mm/s. At each flow speed, 60 original speckle images were obtained using CCD.

B. CALCULATION PRINCIPLE OF LASER SPECKLE CONTRAST RATIO

In general, the statistical quantification standard used for quantitative description uses the coefficient of variation

in statistical methods, which is the speckle contrast ratio K [9], [10], [23]. K is defined as the ratio of the standard deviation of light intensity $\boldsymbol{\sigma_I}$ and the average value $\boldsymbol{I}$ represented by the gray values of all the pixels in the selection window:

$$K = \frac{\sigma_I}{I} \tag{1}$$

The value of the contrast ratio K is in the range of zero–one and describes the relative speed in the original image. K is negatively correlated with the speed of motion of the scattering material.

The relationship between K and the electric field correlation function can be derived using the electric field autocorrelation function, light intensity autocorrelation function, and Siegert relationship between the two. This is shown in Eq. (2):

$$K = \sqrt{\beta \frac{e^{-2x} - 1 + 2x}{2x^2}} \tag{2}$$

Among these, β is a stable system parameter and is generally omitted or defaulted to one, $x = T/\tau c$, T is the exposure time of the CCD camera, erf is the standard error, and τc is the decorrelation time of the light intensity representing the speed of motion of the scattered particles.

The motion state of the scattered particles is highly complex. For example, the motion of blood cells in a blood vessel has a directional movement, and in addition, the cells deform and rotate. Therefore, it is difficult to obtain an accurate relationship between the speed of the scattered material and velocity of the measured liquid in the flow direction. It is more difficult to obtain the absolute velocity of the scattered material. Therefore, the relative variation in the flow velocity is more frequently used for comparison.

Assuming that an image has M × N pixels, the CCD camera can read the gray value I(x,y) at any point (x,y) in the image. Thus, the speckle image is expressed as Eq. (3):

$$F = I(x, y) \tag{3}$$

The image is processed according to the speckle definition (Formula 1). For an N × N-sized space sliding window with (x',y') as the center pixel, Eq. (6) is obtained using Eq. (4) and Eq. (5):

$$\bar{I}(x', y') = \frac{\sum_{a=-m/2}^{m/2} \sum_{b=-m/2}^{m/2} I(x+a, y+b)}{m^2} \tag{4}$$

$$\sigma(x', y') = \sqrt{\frac{\sum_{a=-m/2}^{m/2} \sum_{b=-m/2}^{m/2} I(x+a, y+b-\bar{I})^2}{m^2}} \tag{5}$$

$$K_s(x', y') = \frac{\sigma(x', y')}{\bar{I}(x', y')} \tag{6}$$

The contrast value of the corresponding sub-image was calculated using the above-mentioned formula. This contrast value was then used as the value of the image center point to traverse the entire image and to obtain the contrast map corresponding to the original image.

C. INTRODUCTION OF IMAGE ENTROPY

Image entropy is a form of image feature statistic introduced into the image field by information entropy. It is an estimated value that represents the degree of image "fuzziness." It reflects the average amount of information in the image and is a feature quantity that describes the degree of image blur [23], [25]–[27]. The formula for calculating the image entropy of a discrete two-dimensional image is

$$H = \sum_{i=0}^{255} p_i log p_i \tag{7}$$

In the above formula, p_i is the probability of each gray level in the selected area.

Image entropy reflects the aggregation characteristics of the image gray distribution, whereas it cannot reflect its spatial characteristics. Based on the amount of information contained in the image, the two-dimensional entropy of the image can reflect the gray information of the pixel position in the image and the comprehensive characteristics of the gray distribution in the pixel neighborhood. Furthermore, it has high stability and strong anti-interference capability [28], [29]. The formula for calculating the two-dimensional entropy of the image is

$$H = \sum_{i=0}^{255} p_{ij} log p_{ij} \tag{8}$$

where $p_{i,j} = f(i,j)/(N \times M)$, i is the gray value of the pixel, j represents the average gray value of its domain, and N and M are scales of the selected area image.

The result of the one-dimensional entropy is similar to contrast calculation. The results obtained at each time are independent of each other. As a result, there are deficiencies in contrast resolution and contrast accuracy. Thus, two-dimensional entropy was introduced in this study to calculate the feature of the image background based on the quantity. In addition, the E-LSCI algorithm used this as a supplementary correction method in contrast calculation, to propose an improved contrast calculation method.

$$K_{2De} = K_S \times \frac{c}{e^H} \tag{9}$$

where K_s is the contrast ratio obtained by the calculation of the original image, H is the two-dimensional entropy obtained by the calculation of the background part of the original image area, and c is a constant for normalizing e^H.

D. CONTRAST ACCURACY A_E AND CONTRAST RESOLUTION R_E

This study used statistically obtained normal distribution $f(x; \mu, \sigma) = 1/(\sigma\sqrt{2\pi})\exp(-((x-\mu) \wedge 2)/(2\sigma \wedge 2))$. The variance σ and mean u were used as the basis to evaluate the accuracy of the analysis of the speckle image contrast value. The correctness of the contrast statistical histogram sequence calculated at different speeds was used to quantitatively study the contrast accuracy of the current algorithm at m flow rates A_e:

$$A_e = \frac{1}{m \times (m-1)} \sum_{i=1}^{m} \sum_{j=1}^{m} G_{i,j} \tag{10}$$

where $G_{i,j}$ is the comparison results of the contrast ratio of the flow velocity of i to that of j:

$$G_{i,j} = \begin{cases} 1, & (i-j)(u_j - u_j) < 0 \\ 0, & (i-j)(u_j - u_j) \geq 0 \end{cases} \tag{11}$$

To evaluate the resolution of the contrast value of the speckle image, the statistical results of the contrast ratio corresponding to different speeds were used, and the area overlap degree of the normal distribution map of the contrast statistics obtained was used to quantify the contrast resolution $R_{i,j}$ of the current algorithm. Thereby, we could count the distinguishable degree of a certain flow velocity that does not overlap with other flow velocity regions. This is expressed as:

$$\begin{aligned} R_{i,j} &= \frac{3 \times (\sigma_i + \sigma_j) + (u_i - u_j) - (6 \times (\sigma_i + \sigma_j) - (3 \times (\sigma_i + \sigma_j) + (u_i - u_j)))}{6 \times (\sigma_i + \sigma_j)} \\ &= \frac{(u_i - u_j)}{3 \times (\sigma_i + \sigma_j)} \end{aligned} \tag{12}$$

Owing to the 68–95–99.7 rule, three times the variance could represent 99.73% of the statistical data, and factor six is the statistic of the area covered by the normal distribution.

Therefore, the common contrast resolution R_e of m flow rates is as follows:

$$R_e = \frac{2}{m \times (m-1)} \sum_{i=1}^{m-1} \sum_{j=i+1}^{m} R_{i,j} \tag{13}$$

where $\sigma_i, \sigma_j, u_i,$ and u_j are the variances and mean values, respectively, of two velocities. Among these, the flow rate resolution of the incorrect velocity sorting $R_{i,j} < 0$ is assessed to be zero, and $R_{i,j} > 1$ indicates that the areas occupied by the two flow rates do not overlap each other. At this time, it is determined that $R_{i,j} = 1$.

The higher the accuracy A_e, the higher is the precision of the current contrast result. The higher the resolution R_e, the higher is the discriminant of the contrast result.

In addition, the correlation between the flow speed and contrast ratio was studied and expressed by the correlation coefficient. Correlation is a non-deterministic relationship, and the correlation coefficient is a measure of the degree of linear correlation between variables. This relationship is expressed as follows:

$$r(X, Y) = \frac{Cov(X, Y)}{\sqrt{Var[X]Var[Y]}} \tag{14}$$

where $Cov(X, Y)$ is the covariance of X and Y, $Var[X]$ is the variance of X, and $Var[Y]$ is the variance of Y.

III. EXPERIMENTAL RESULTS AND DISCUSSION

A. STANDARD TEST AND ANALYSIS METHODS

In Fig. 2 (a), the original image data obtained for the experiment (a gray-scale contrast enhanced image) were selected from the original image, and the two-dimensional entropy on the background was calculated from the background region. The original image on which the traditional LSCI method

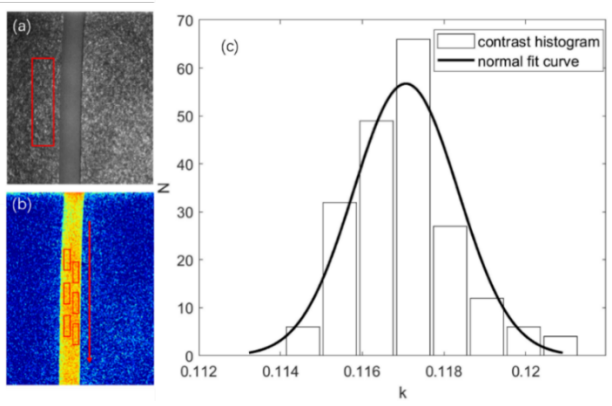

FIGURE 2. Statistical analysis diagram of hose experiment: (a) original image (contrast-stretched), the red rectangle is the background selection area; (b) traditional contrast result (pseudo-color image), the red rectangle is the randomly selected lining in the tube ratio statistics area, and the red arrow is the direction of liquid flow; (c) current image contrast ratio statistical histogram and normal fitting curve.

was applied to obtain pseudo-color imaging results are shown in Fig. 2 (b). A statistical analysis was performed on the average contrast ratio of selected small areas in the hose to obtain the statistical histogram of the contrast ratio at this flow (1.2 mm/s) speed and its normal distribution diagram. The normal distribution diagram of a single flow speed in the hose is shown in Fig. 2(c). The contrast accuracy and contrast resolution between different flow speeds and contrast ratios were analyzed through the normal fitting curve of the calculated contrast ratio.

A randomly selected set of five original contrast distributions of different flow velocities are shown in Fig. 3 (a). Here, the sequence numbers 1–5 refer to the flow velocity that varies from 0.4 to 1.2 mm/s at intervals of 0.2 mm/s. Fig. 3(b) is a contrast distribution plot obtained using the E-LSCI algorithm for this set of data.

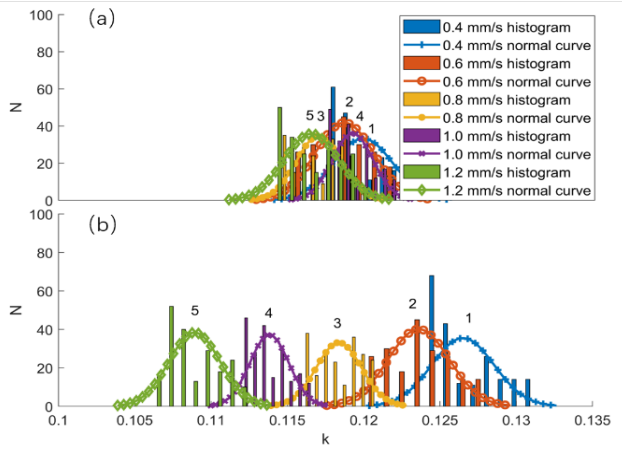

FIGURE 3. Contrast ratio distribution diagram at different flow speeds: (a) LSCI and (b) E-LSCI algorithm.

Based on the evaluation criteria of contrast resolution and contrast accuracy, five contrast ratios corresponding to

different speeds were correctly identified according to the criterion that a larger speed results in a smaller contrast ratio (see Fig. 3 (a)). The accuracy $A_e = 0.8$ and contrast resolution $R_e = 0.1459$ were identifiable by the contrast corresponding to different speeds. The results show that the traditional contrast calculation method is vulnerable to errors in the flow velocity and contrast value. This is because it has time specificity unique to it for each instant of the original speckle image, which weakens the analog capability of the contrast in the calculation of the laser speckle flow velocity. This may result in a scenario where the contrast ratio corresponding to the flow velocity is higher when the flow speed is faster and the contrast ratio accuracy is low. Alternatively, the contrast ratio sections of different flow speeds overlap each other, and the contrast ratio resolution is low.

After a recalculation of the E-LSCI algorithm, the same set of images was analyzed with different flow speeds. The results are shown in Fig. 3 (b). The contrast accuracy was $A_e = 1$, the contrast resolution was $R_e = 0.7598$, the flow speeds were arranged in a more correct order, and the resolution between the different flow speeds in Fig. 3 (a) was improved significantly. For this group of images, the E-LSCI algorithm improved the contrast accuracy and contrast resolution by 25% and 420%, respectively. The E-LSCI algorithm significantly improved the correlation between flow velocity and contrast.

B. METHOD VALIDATION EXPERIMENT AND ANALYSIS

According to the aforementioned analysis method, the 60 original speckle images obtained with each of the nine liquid flow speeds were combined. In this paper, one picture is randomly selected from each different flow rate, and the 9 pictures are combined and analyzed. The selected pictures are not put back into the original data, and 60 groups of data are obtained for analysis. We used LSCI, laser speckle background mean contrast imaging (LSMCI), and E-LSCI sequentially to analyze these 60 groups of images and obtained the contrast accuracy analysis shown in Fig. 4.

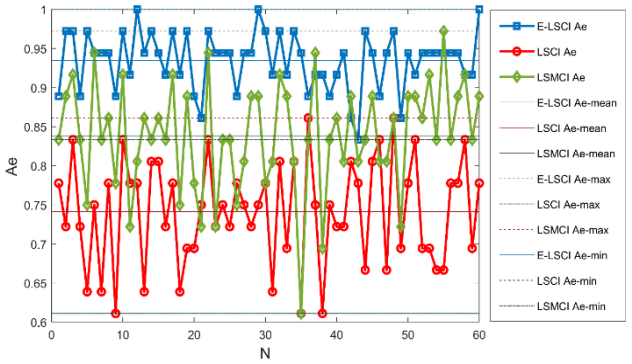

FIGURE 4. Accuracy statistics diagram of LSSCI, LSMCI, and E-LSCI algorithms.

As shown in Fig. 4, maximum, minimum, and average contrast accuracies of $A_{emax} = 0.8611$, $A_{emin} = 0.6111$, and $A_{emean} = 0.7412$, respectively, were obtained for a group of images using LSCI. In addition, the variance of the contrast accuracy of all the combinations was 0.0670. The contrast accuracy obtained by LSMCI is shown by the green line in Fig. (4). Here, $A_{emax} = 0.9722$, $A_{emin} = 0.6111$, $A_{emean} = 0.8384$, and the variance of the contrast accuracy for all the combinations is 0.0700. The variance result is marginally larger than that of the LSCI method. However, 80% of the random combinations of different speeds in the contrast ranking have a contrast accuracy improvement of over 20% compared with the LSCI method. The contrast accuracy obtained is shown by a blue line in Fig. 4. The contrast value obtained using the E-LSCI algorithm improved the contrast accuracy of each group. Among the groups, three groups of E-LSCI algorithms for contrast arrangement achieved the maximum contrast accuracy $A_{emax} = 1$. This implies that the correct sorting degree was 5% and that the minimum and average contrast accuracies were $A_{emin} = 0.8333$ and $A_{emean} = 0.9347$. From the different speeds, 80% that were combined randomly in the contrast sorting attained a contrast accuracy of over 90%. Fig. 4 and the variance results reveal that the contrast accuracy of LSCI was not high at marginal flow-speed differences and that the degree of fluctuation was large. However, the contrast accuracy of the E-LSCI algorithm was high and relatively stable.

The comparison results of the accuracies of the LSCI, LSMCI, and E-LSCI methods in the study show that E-LSCI improves the contrast accuracy of LSCI by more than 27%; the same, compared to LSMCI method improves the contrast accuracy to a higher degree. Furthermore, the result was less fluctuating, and the resolution effect was better. This shows that the application of the E-LSCI method can effectively improve the contrast accuracy.

As shown in Fig. 5, maximum, minimum, and average resolutions of $R_{emax} = 0.3794$, $R_{emin} = 0.1361$, and $R_{emean} = 0.2528$, respectively, were obtained for a group of images using LSCI. Its variance was 0.0554, the overlap between different flow speeds was very high, and the resolution capability was exceptionally weak.

The contrast resolution of each group (calculated using the LSMCI algorithm) was improved. This is shown by the green line in Fig. 5. The maximum, minimum, and average resolutions were $R_{emax} = 0.4120$, $R_{emin} = 0.0.1698$, and $R_{emean} = 0.0.2755$, respectively, and its variance was 0.0547. The degree of overlap between different flow speeds is significantly high, and the resolving power is close to that of LSCI.

The contrast resolution of each group (calculated using the E-LSCI algorithm) was improved. This is shown by the blue line in Fig. 5. The maximum, minimum, and average resolutions were $R_{emax} = 0.8611$, $R_{emin} = 0.6111$, and $R_{emean} = 0.7412$, respectively, and its variance was 0.0423. A total of 100% of the combinations achieved a resolution of over 60%. The capability to distinguish between different flow speeds and contrast ratios was evident.

As shown in Fig. 5, the contrast resolution of LSCI and M-LSCI in the contrast ratio of different flow speeds under

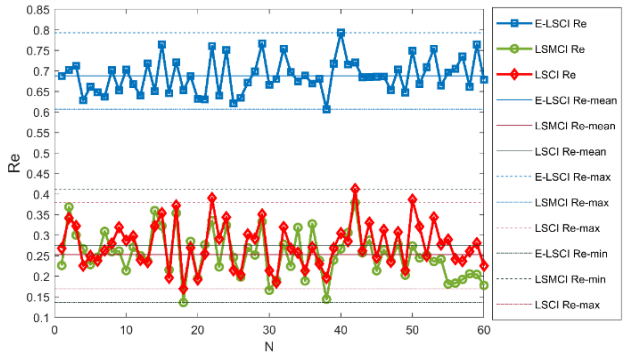

FIGURE 5. Resolution statistics of LSCI, LSMCI, and E-LSCI algorithms.

the condition of marginal flow-speed difference was moderate. The contrast ratio obtained in the corresponding results was also moderate. Furthermore, the degree of fluctuation was large, whereas the contrast resolution of the E-LSCI algorithm was higher and more stable.

The average effect of the E-LSCI algorithm on the accuracy of LSCI was 184% of the E-LSCI results, and the highest increase was 379%. The resolution of the E-LSCI algorithm was based on the LSCI, and there was a significant improvement in the resolution.

The distribution of the contrast ratio with flow velocity determined through a comprehensive statistical analysis of 60 groups of original images is shown in Fig. 6. For LSCI, although the contrast ratio decreased with an increase in the overall speed, the obtained correlation to the overall mean was −0.7478, the contrast ratio was negative at different speeds, and the flow speed difference was smaller. The degree of correlation was also reduced significantly. The correlation degree between the flow speed and the contrast ratio was 0.0828 for a flow speed above 0.9 mm/s. The speed and contrast ratio tended to be positively correlated, and the resolution was low. It was difficult to distinguish different speeds

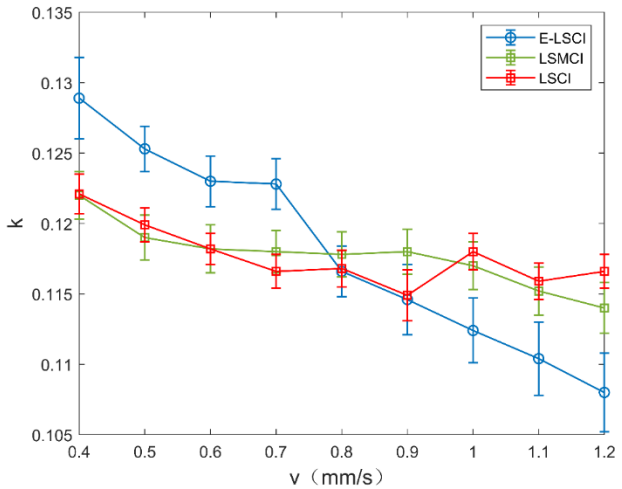

FIGURE 6. Overall tendency of contrast ratio with flow velocity.

using contrast ratio as a measure. For the LSCI, the calculation results for high flow speeds were ineffective. There were large fluctuations in the value of the corresponding contrast ratio under different flow speeds. Even the accuracy and resolution were low, which hindered the attainment of more accurate results.

LSMCI is similar to LSCI. The correlation between the mean value of the overall contrast ratio and flow speeds is −0.9462. However, the distinguishability of the contrast ratio is reduced significantly when the speed is different and the flow speed difference is marginal. Moreover, although the flow velocity contrast ratio in the interval 0.6 mm/s–0.9 mm/s has a negative correlation, it is essentially on the same horizontal line. Furthermore, it is difficult to display the distinguishing effect. At this time, the distinguishing capability of LSMCI is low, and it is difficult to distinguish different speeds using the metric value of the contrast ratio. For LSMCI, when the flow speed difference is marginal, the relative results calculated between different flow speeds are relatively ineffective. Furthermore, a scenario occurs where the corresponding contrast ratio numbers are closer to the corresponding contrast ratio values at different flow speeds, and it is difficult to obtain more accurate results.

For E-LSCI, the larger the overall speed, the smaller is the contrast ratio. The correlation between the mean value of the overall contrast ratio and flow speed was -0.9901, and the overall tendency was to attain a negative linear relationship and higher stability. For an identical experimental system, the E-LSCI algorithm expanded the measurement range. However, the accuracy with which the E-LSCI method obtained the contrast ratio near the flow speed of 0.7 mm/s was low. Moreover, the error degree of 0.7 mm/s was higher for the accuracy obtained when the flow speed was arranged in sequence. It is likely that the current E-LSCI algorithm has a weak recognition capability in this flow speed range.

C. FINGER OBSTRUCTION TEST (EXAMPLE TEST)

In Fig. 7, for the pseudo-color image of a finger captured with the current laser speckle system and calculated

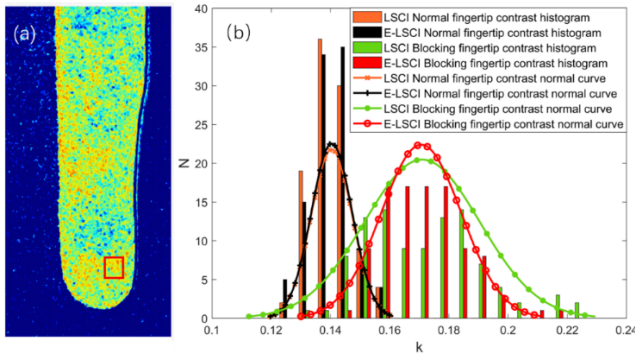

FIGURE 7. (a) Contrast map of finger obstruction experiment (the red area is the selected contrast area), (b) E-LSCI algorithm and LSCI calculation statistics of fingertip contrast ratio.

contrast, the fingertip region (25 × 25 pixels) was selected as the area of interest for the analysis. The finger experiment was divided into two stages. First, the finger in the normal relaxation state was photographed. After 30 s, the finger in the blockage state was photographed. Two sets of images were captured, with 100 images captured at intervals of 1 s for each set. The previous method verification revealed that LSMCI had yielded ineffective results. Only the LSCI and E-LSCI method analysis were applicable here.

Figure 7(b) shows the histogram statistics and normal fitting curve of the final contrast results of the LSCI and E-LSCI algorithms for the two experimental processes. The area occupied by the contrast histograms obtained by E-LSCI and LSCI in the normal relaxed state of the finger and in its blocked state is relatively wide. This is owing to the large randomness of the flow velocity generated by the complex flow of blood microcirculation in the finger. The contrast statistics obtained by the two methods (E-LSCI and LSCI) in the normal relaxed state of the fingers had evident variations. Meanwhile, the contrast histogram obtained by E-LSCI in the blocked state was more concentrated than that obtained by LSCI. The contrast display results for the finger were better in the blocked state. However, the contrast interval corresponding to the flow velocity of the LSCI and E-LSCI algorithms did not fluctuate significantly, and the final average values obtained closer to each other

Table 1 shows the statistics of fingertip contrast calculation for E-LSCI and LSCI. It can be observed from the table that the average of the two contrast algorithms is essentially identical. This is because the E-LSCI algorithm normalizes the final results during the calculation, which enhances the stability of the E-LSCI algorithm. The range of the E-LSCI algorithm is 25.5%, which is better than that of LSCI. The reduction in the range shows that the E-LSCI algorithm has a good effect on the elimination of the abnormal results at an identical flow rate. The standard deviation of the E-LSCI algorithm is 26.8%, which is lower than that of the LSCI algorithm. This reveals that the E-LSCI algorithm reduces the dispersion of the contrast ratio at an identical flow velocity and enhances the stability of the contrast results.

TABLE 1. E-LSCI and LSCI calculation table for fingertip contrast ratio.

Name	Mean	Range	Std
LSCI normal fingertip contrast	0.1404	0.0360	0.0070
E-LSCI normal fingertip contrast	0.1404	0.0357	0.0069
LSCI blocking fingertip contrast	0.1770	0.0941	0.0195
E-LSCI blocking fingertip contrast	0.1707	0.1701	0.0135

The effect of E-LSCI is not apparent for the normal fingertips and for enhancing the stability of the contrast. It is likely that there is still a natural variation in the flow rate of the microcirculation during the photography, which causes the flow rate of the contrast to be unstable and thereby, the contrast to fluctuate substantially. The contrast resolution of the two state E-LSCI algorithms for the fingertip is Re = 0.4928, whereas the resolution of LSCI is 0.3848. For these two flow rate E-LSCI algorithms, the improvement was 25%, and the effect was still significant for the two corresponding contrast E-LSCI algorithms with an apparent flow rate difference.

IV. SUMMARY

From the above analysis, the contrast analysis error could be eliminated using the contrast optimization algorithm based on two-dimensional entropy in the LSCI technique (2DE-LSCI). In the standard experiment, the data revealed that compared with LSCI, the current E-LSCI algorithm improved the contrast accuracy by 20%–50%, and it enhanced the accuracy of the flow velocity of the measurement system. Moreover, for the same measurement system, the current algorithm enlarged the measurement range of the system and enhanced its applicable range. In the finger blocking experiment, the contrast resolution of the E-LSCI algorithm was 25% higher than that of the LSCI algorithm. The example of a blocking experiment shows that the algorithm is effective.

This paper explores the blood flow microcirculation of 2DE-LSCI technology in the physiological measurement and health state of organisms. Due to the limitation of current experimental conditions, the amount of data collection is small, which may not cover more age groups and whether the body is healthy or not. In the later research, we should expand the collection data set and analyze the relationship between blood microcirculation and physiological state through a large number of data.

REFERENCES

[1] A. Humeau-Heurtier, M. A. Colominas, G. Schlotthauer, M. Etienne, L. Martin, and P. Abraham, "Bidimensional unconstrained optimization approach to EMD: An algorithm revealing skin perfusion alterations in pseudoxanthoma elasticum patients," *Comput. Methods Programs Biomed.*, vol. 140, pp. 233–239, Mar. 2017.

[2] K. He, S. Huang, and X. Qian, "Early detection and risk assessment for chronic disease with irregular longitudinal data analysis," *J. Biomed. Informat.*, vol. 96, Aug. 2019, Art. no. 103231.

[3] H. Jiang, Y. Liu, Y. Wei, Y. Shi, C. B. Wright, X. Sun, T. Rundek, B. S. Baumel, J. Landman, and J. Wang, "Impaired retinal microcirculation in patients with Alzheimer's disease," *PLoS ONE*, vol. 13, no. 2, 2018, Art. no. e0192154.

[4] V. Via and V. N. Blokhin, "Disorders of microcirculation in patients with acute surgical diseases of the biliary tract," *Therapeutic Arch.*, vol. 56, no. 8, pp. 122–125, 1984.

[5] H. A. J. Struijker-Boudier, A. E. Rosei, P. Bruneval, P. G. Camici, F. Christ, D. Henrion, B. I. Lévy, A. Pries, and J.-L. Vanoverschelde, "Evaluation of the microcirculation in hypertension and cardiovascular disease," *Eur. Heart J.*, vol. 28, no. 23, p. 2834, 2007.

[6] A. R. Chade and J. E. Hall, "Role of the renal microcirculation in progression of chronic kidney injury in obesity," *Amer. J. Nephrol.*, vol. 44, no. 5, pp. 354–367, 2016.

[7] A. J. Deegan and R. K. Wang, "Microvascular imaging of the skin," *Phys. Med. Biol.*, vol. 64, no. 7, Mar. 2019, Art. no. 07TR01.

[8] J. Horstmann, H. Spahr, C. Buj, M. Münter, and R. Brinkmann, "Full-field speckle interferometry for non-contact photoacoustic tomography," *Phys. Med. Biol.*, vol. 60, no. 10, pp. 4045–4058, May 2015.

[9] A. Seeck *et al.*, "Correlation between autonomic dysfunction and impaired microcirculation in patients with schizophrenia," *Biomed. Eng.*, vol. 58, no. SI-1-Track-G, 2013, Art. no. 000010151520134174.

[10] M. Chen, D. Wen, S. Huang, S. Gui, Z. Zhang, J. Lu, and P. Li, "Laser speckle contrast imaging of blood flow in the deep brain using microendoscopy," *Opt. Lett.*, vol. 43, no. 22, pp. 5627–5630, 2018.

[11] O. Yang, D. Cuccia, and B. Choi, "Real-time blood flow visualization using the graphics processing unit," *J. Biomed. Opt.*, vol. 16, no. 1, 2011, Art. no. 016009.
[12] J. D. Briers, "Laser Doppler, speckle and related techniques for blood perfusion mapping and imaging," *Physiol. Meas.*, vol. 22, no. 4, pp. 35–66, 2001.
[13] D. Jakovels, I. Saknite, and J. Spigulis, "Implementation of laser speckle contrast analysis as connection kit for mobile phone for assessment of skin blood flow," *Proc. SPIE*, vol. 9129, pp. 91293I-1–91293I-8, May 2014.
[14] D. Jakovels, I. Saknite, G. Krievina, J. Zaharans, and J. Spigulis, "Mobile phone based laser speckle contrast imager for assessment of skin blood flow," *Proc. SPIE*, vol. 9421, Oct. 2014, Art. no. 94210J.
[15] A. Pérez, R. González-Peña, R. Braga, Jr., Á. Perles, E. Pérez–Marín, and F. García-Diego, "A portable dynamic laser speckle system for sensing long-term changes caused by treatments in painting conservation," *Sensors*, vol. 18, no. 2, p. 190, Jan. 2018.
[16] L. Zhang, L. Ding, M. Li, X. Zhang, D. Su, J. Jia, and P. Miao, "Dual-wavelength laser speckle contrast imaging (dwLSCI) improves chronic measurement of superficial blood flow in hands," *Sensors*, vol. 17, no. 12, p. 2811, Dec. 2017.
[17] H. He, Y. Tang, F. Zhou, J. Wang, Q. Luo, and P. Li, "Lateral laser speckle contrast analysis combined with line beam scanning illumination to improve the sampling depth of blood flow imaging," *Opt. Lett.*, vol. 37, no. 18, pp. 3774–3776. 2012.
[18] W. Cheng, X. Zhu, X. Chen, M. Li, J. Lu, and P. Li, "Manhattan distance-based adaptive 3D transform-domain collaborative filtering for laser speckle imaging of blood flow," *IEEE Trans. Med. Imag.*, vol. 38, no. 7, pp. 1726–1735, Jul. 2019.
[19] T. Oliver, A. Michael, and H. Evan, "Correction for spatial averaging in laser speckle contrast analysis," *Biomed. Opt. Exp.*, vol. 2, no. 4, pp. 1021–1029. 2011.
[20] J. C. Ramirez-San-Juan, E. Mendez-Aguilar, N. Salazar-Hermenegildo, A. Fuentes-Garcia, R. Ramos-Garcia, and B. Choi, "Effects of speckle/pixel size ratio on temporal and spatial speckle-contrast analysis of dynamic scattering systems: Implications for measurements of blood-flow dynamics," *Biomed. Opt. Exp.*, vol. 4, no. 10, pp. 1883–1889, 2013.
[21] H. Cheng, Q. Luo, S. Zeng, S. Chen, J. Cen, and H. Gong, "Modified laser speckle imaging method with improved spatial resolution," *J. Biomed. Opt.*, vol. 8, no. 3. pp. 559–564, 2003.
[22] A. Humeau-Heurtier, G. Mahe, S. Durand, and P. Abraham, "Multiscale entropy study of medical laser speckle contrast images," *IEEE Trans. Biomed. Eng.*, vol. 60, no. 3, pp. 872–879, Mar. 2013.
[23] P. Miao, Z. Chao, Y. Zhang, N. Li, and N. V. Thakor, "Entropy analysis reveals a simple linear relation between laser speckle and blood flow," *Opt. Lett.*, vol. 39, no. 13, pp. 3907–3910, 2014.
[24] R. Zhang, L. Song, J. Xu, X. An, W. Sun, X. Zhao, Z. Zhou, and L. Chen, "Laser speckle imaging for blood flow based on pixel resolved zero-padding auto-correlation coefficient distribution," *Opt. Commun.*, vol. 439, pp. 38–46, May 2019.
[25] D. Briers, D. D. Duncan, E. Hirst, S. J. Kirkpatrick, M. Larsson, W. Steenbergen, T. Stromberg, and O. B. Thompson, "Laser speckle contrast imaging: Theoretical and practical limitations," *J. Biomed. Opt.*, vol. 18, no. 6, Jun. 2013, Art. no. 066018.
[26] Z. Z. Tao, L. S. Fa, and C. H. Ping, "Research on auto-focused function based on the image entropy," *Opt. Precis. Eng.*, vol. 12, no. 5, pp. 537–544, 2004.
[27] Y. Chen, D. Xu, and Q. Li, "Descriptive method for image stability based on entropy," *Chin. J. Sci. Instrum.*, vol. 27, no. 3, pp. 2121–2122, 2006.
[28] L. E. V. Silva, A. C. S. S. Filho, V. P. S. Fazan, J. C. Felipe, and L. O. M. Junior, "Two-dimensional sample entropy: Assessing image texture through irregularity," *Biomed. Phys. Eng. Exp.*, vol. 2, no. 4, Jul. 2016, Art. no. 045002.
[29] A. O. Pei *et al.*, "Combination of morphological filtering method based on 2-D entropy and application," *CEA*, vol. 51, no. 6, pp. 163–166, 2015.

XINGLONG LIU received the B.S. degree from Zhengzhou University, in 2019. He is currently pursuing the M.S. degree with the University of Shanghai for Science and Technology. His research interest includes biomedical imaging.

HUI YANG received the Ph.D. degree in optical engineering from the University of Shanghai for Science and Technology (USST), in 2009. He joined the School of Optical-Electrical and Computer Engineering, USST, in 2009. His research interests include particle technology, photoelectric precision detection, and digital image processing.

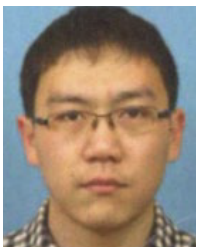

RAN LI received the bachelor's degree in communication engineering from Henan Normal University, in 2012, and the Ph.D. degree in optical engineering from the University of Shanghai for Science and Technology, in 2019. Since July 2019, he has been working as a Postdoctoral Fellow in biomedical engineering with the University of Shanghai for Science and Technology. His research interests include high-precision optical measurement and granular matter.